Publication IV

Leena Nurmi, Hui Peng, Jukka Seppälä, David M. Haddleton, Idriss Blakey, and Andrew K. Whittaker. 2010. Synthesis and evaluation of partly fluorinated polyelectrolytes as components in $^{19}F$ MRI-detectable nanoparticles. Polymer Chemistry, volume 1, number 7, pages 1039-1047.

# Synthesis and evaluation of partly fluorinated polyelectrolytes as components in $^{19}$F MRI-detectable nanoparticles†

Leena Nurmi,[a] Hui Peng,[b] Jukka Seppälä,[a] David M. Haddleton,[c] Idriss Blakey[b] and Andrew K. Whittaker*[b]

*Received 2nd February 2010, Accepted 15th April 2010*
**DOI: 10.1039/c0py00035c**

A series of partly fluorinated polyelectrolytes were synthesized by transition metal mediated living radical polymerization and evaluated for their applicability as corona-forming components in $^{19}$F MRI-detectable nanoparticles in aqueous solutions. The polymers were statistical and block copolymers of trifluoroethyl methacrylate (TFEMA) and 2-(dimethylamino)ethyl methacrylate (DMAEMA). The polymers were either directly dissolved in water (statistical copolymers), or assembled into aqueous nanoparticles with PTFEMA cores and P(TFEMA-*co*-DMAEMA) coronas (block copolymers). The polymer composition, polymer charge density, solution ionic strength and solution pH were varied. The $^{19}$F spin–lattice ($T_1$) and spin–spin ($T_2$) relaxation times and $^{19}$F image intensities of solutions of the polymers were measured and related to polymer structure and aqueous conformation. The $^{19}$F NMR $T_2$ relaxation times were found to be highly indicative of the $^{19}$F imaging performance. Maintaining sufficient mobility of the $^{19}$F nuclei was important for obtaining images of high intensity. $^{19}$F mobility could be increased by preventing their aggregation in water by exploiting electrostatic repulsion between monomer units.

## Introduction

Recently, there has been growing interest in the development of fluorinated compounds capable of being tracked *in vivo* using $^{19}$F magnetic resonance imaging ($^{19}$F MRI). With the advent of commercially available $^{19}$F MRI coils, $^{19}$F imaging is achievable in the clinical setting. When the $^{19}$F image is superimposed on the familiar $^{1}$H density image, the location of a fluorinated compound, *e.g.* therapeutic particle or cell, can be determined in a non-invasive manner. $^{19}$F is an attractive tracking nucleus for MRI due to its high sensitivity and the absence of a confounding $^{19}$F background signal within the body.

The requirements for a successful $^{19}$F MRI tracking agent include that it should have a high fluorine content, the fluorine nuclei should have appropriate NMR properties as discussed below, and preferably there should be a single peak in the $^{19}$F NMR spectrum. Such compounds have the potential to provide high image intensity without the need for selective excitation sequences. A variety of fluorinated compounds have been studied, ranging from small fluorocarbon molecules[1] to oligomeric emulsions[2] and quite recently, to polymeric nanoparticles and particulates.[3–7] The targeted applications have varied on a broad scale, including a multitude of *in vivo* experiments. For example, Higuchi *et al.*[8] have reported the imaging of fluorinated amyloidophilic compounds in living mice as potential markers for the early stages of Alzheimer's disease, and Janjic *et al.*[2] have visualized the migration of T-cells loaded with oligomeric perfluoropolyether (PFPE) emulsions.

Fluorinated polymeric nanoparticles have recently received attention as potential $^{19}$F MRI tracking compounds, as they have large structural design potential when compared to traditional systems such as emulsions and solutions of smaller molecules. The diversity of polymeric structures achievable with modern synthetic methods allows the incorporation of a multitude of fluorine nuclei within a nanoparticle, potentially leading to high image intensity. However, the hydrophobic nature of fluorinated groups makes them susceptible towards aggregation in water, and the resulting reduction in molecular mobility can lead to loss of signal intensity. Specifically, the spin–spin relaxation time ($T_2$) of polymeric nuclei is heavily influenced by local motions, with nuclei in constrained environments exhibiting faster $T_2$ relaxation, and therefore broader signals having poorer signal-to-noise ratio (SNR), than identical nuclei in less-constrained environments.[9]

A number of studies have been published on $^{19}$F MRI of polymeric nanoparticles. Du *et al.*[3,4] formed particles by grafting poly(acrylic acid-*co*-trifluoroethyl methacrylate) copolymer coronas from a small hydrophobic core. They conducted phantom $^{19}$F MRI and relaxation time measurements of the aqueous particle solutions, and observed that the $T_2$ of the fluorine nuclei was reasonably long ($T_2$ = 50–56 ms) and the particles were detectable by $^{19}$F MRI. Nyström *et al.*[6] formed particles from poly(acrylic acid)-*b*-poly(styrene-*co*-pentafluorostyrene) block copolymers. In this study, the

[a]*Department of Biotechnology and Chemical Technology, Aalto University, PL 16100, 00076 Aalto, Finland. E-mail: leena.nurmi@tkk.fi*
[b]*Australian Institute for Bioengineering and Nanotechnology, The University of Queensland, St Lucia, 4072, Australia. E-mail: a.whittaker@uq.edu.au; Fax: +61-7-33463973; Tel: +61-7-3346388*
[c]*Department of Chemistry, University of Warwick, Coventry, CV4 7AL, UK*

† Electronic supplementary information (ESI) available: (1) Experimental details for the synthesis of block copolymers of TFEMA and DMAEMA. (2) Experimental details for the synthesis of statistical copolymers of TFEMA and DMAEMA. (3) Detailed polymerization results for TFEMA/DMAEMA block and statistical copolymers. (4) Reactivity ratio measurements of the DMAEMA/TFEMA monomer pair. (5) The exponential decay curves of the spin–spin ($T_2$) relaxation time measurements. See DOI: 10.1039/c0py00035c

fluorine nuclei were incorporated within the hydrophobic core-forming block, and it was noticed that no $^{19}F$ signal could be detected from the aqueous particle solution. This indicated that the rigid core significantly restricted the mobility of the core nuclei. Peng *et al.*[5] formed nanoparticles from block copolymers of poly(acrylic acid) with varying fluorinated hydrophobic blocks. Again, the $^{19}F$ nuclei were incorporated within the cores of the particles. However, in this case it was noticed that by lowering the glass transition temperature ($T_g$) of the core by choosing low $T_g$ components, detectable $^{19}F$ signal could be obtained from the aqueous nanoparticle solutions. The longest $T_2$ and highest phantom image intensity were obtained with particles of poly(acrylic acid)-*b*-poly(trifluoroethyl acrylate-*co*-butyl acrylate) block copolymers ($T_2 = 1.75$ ms).

The previous studies of nanoparticle systems with $^{19}F$ nuclei within the coronas of the particles have shown promising results.[3,4] To further improve the imaging performance of such particles, the $^{19}F$ content in the corona could be increased in order to obtain higher image intensity. However, increasing the $^{19}F$ density also increases the hydrophobicity of the corona, eventually resulting in aggregation and loss of signal intensity. Our hypothesis is that, in the case of water-soluble polymers (*i.e.* nanoparticles stabilized by fluorinated hydrophilic coronas), the highest $^{19}F$ MRI intensity will be obtained with polymeric materials that combine high fluorine content and efficient aqueous solvation of the fluorinated segments.

One way to limit the aggregation and increase the mobility of the fluorinated segments in water is copolymerization with charged monomer units. The aqueous conformation of polyelectrolytes containing hydrophobic groups is controlled on one hand by the long-range repulsive electrostatic interactions between charged groups and on the other hand by the short-range attractive hydrophobic interactions between hydrophobic groups. Depending on the relative strengths of these forces, hydrophobic polyelectrolyte chains can adopt various conformations in solution, ranging from fully extended chains to collapsed globules.[10–12] Similarly, particles with relatively hydrophobic polyelectrolyte coronas can have extended or collapsed conformations (Scheme 1).

The balance between the repulsive and attractive interactions in hydrophobic polyelectrolytes in solution is determined by various parameters, including the relative contents of charged and hydrophobic groups, the polymer concentration, solution ionic strength and solution pH. The effects of these parameters on the solution conformation of hydrophobic polyelectrolytes have been widely studied theoretically[13,14] and experimentally.[15–18]

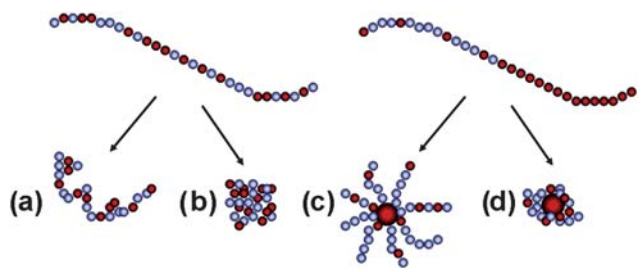


**Scheme 1** Possible conformations in aqueous solutions of hydrophobic polyelectrolytes (left) and block polyelectrolytes assembled to nanoparticles (right). (a) Extended coil, (b) compact globule, (c) extended nanoparticle and (d) compact nanoparticle.

The conformation of the polymer chains has a large impact on the NMR properties of the polymeric nuclei. Measurements of $T_2$ relaxation times along with other NMR techniques have previously been used as a method of probing the conformational restriction of polymeric segments in solutions.[19–23]

In this current study we have synthesized partially fluorinated polyelectrolytes and evaluated their applicability as $^{19}F$ MRI agents. The main objective of the study was to observe how changes in polymer composition and solution conditions (including pH and ionic strength) affect the aqueous conformation and subsequently $^{19}F$ MRI signal intensity of water-soluble polyelectrolyte chains. The polyelectrolytes examined in this work were both statistical and block copolymers of trifluoroethyl methacrylate (TFEMA) and 2-(dimethylamino)ethyl methacrylate (DMAEMA). The statistical polyelectrolytes were directly dissolved in water, whereas the block polyelectrolytes were assembled into aqueous nanoparticles with kinetically frozen PTFEMA cores and P(TFEMA-*co*-DMAEMA) coronas. The $^{19}F$ spin–lattice ($T_1$) and spin–spin ($T_2$) relaxation times and $^{19}F$ image intensities of solutions of the polymers were measured.

## Experimental

### Materials

Copper(I) bromide (Aldrich, 98%) was purified according to the method of Keller and Wycoff.[24] 2-(Dimethylamino)ethyl methacrylate (DMAEMA) (Aldrich, 98%) and 2,2,2-trifluoroethyl methacrylate (TFEMA) (Fluorochem) were passed through basic alumina to remove the inhibitor. *N*-(*n*-Pentyl)-2-pyridylmethanimine[25] and benzyl 2-bromoisobutyrate[26] were synthesized using methods described in the literature. All the other reagents were of analytical grade and used as received.

### Synthesis of the copolymers

**Synthesis of statistical and block copolymers of TFEMA and DMAEMA.** The polymers were synthesized using CuBr/*N*-(*n*-pentyl)-2-pyridylmethanimine as catalyst and benzyl 2-bromoisobutyrate as initiator in 50 v/v% toluene at 90 °C. The block copolymers were prepared by one-pot sequential polymerization, where PTFEMA block was prepared first and DMAEMA monomer was added at around 80% TFEMA conversion. The block copolymers were purified by removal of traces of PTFEMA homopolymer by acidification of a solution of the crude polymer in THF with diluted HCl (aq), which led to the exclusive precipitation of the PTFEMA/PDMAEMA block copolymer. For experimental details, see ESI†.

**Quaternization of TFEMA/DMAEMA copolymers.** Quaternization of the amine groups of DMAEMA monomer units to form the [2-(methacryloyloxy)ethyl] trimethyl ammonium iodide (METAI) monomer units was carried out using a post-polymerization reaction. The copolymer was dissolved in THF (1 g per 100 ml). A three-fold excess of MeI was added. The reaction was left stirring at ambient temperature overnight. The precipitated product was isolated with centrifugation and purified by

dialysis against water. The polymer was recovered by freeze-drying.

### Characterization

**Polymer composition.** NMR spectra were obtained on a Bruker DPX-400 spectrometer. The molecular weights of the polymers were calculated by comparing the integrals of chain-end signals and appropriate peaks related to the polymer backbone. Molar mass distributions were measured using size exclusion chromatography (SEC). The system consisted of two PL gel 5 μm mixed D columns (300 × 7.5 mm) and one PL gel 5 mm guard column (50 × 7.5 mm), with both DRI and UV (at 250 nm) detection, using THF/triethylamine 95 : 5 v/v at 1.0 ml $min^{-1}$ as the eluent. The system was calibrated with PS standards. The reactivity ratios of TFEMA and DMAEMA were measured by Jaacks method.[27] For details on the measurement of reactivity ratios, see ESI†.

**Differential scanning calorimetry (DSC).** DSC was used to determine the glass transition temperature ($T_g$) of PTFEMA using a Mettler Toledo Star instrument in a nitrogen environment. The sample was heated at 20 °C $min^{-1}$ to 150 °C and then cooled at 20 °C $min^{-1}$ to 0 °C to remove any effects induced by prior treatment. The $T_g$ was then determined by heating from 0 °C to 150 °C at 10 °C $min^{-1}$.

**Dynamic light scattering (DLS).** DLS measurements were performed on a Nanoseries (Malvern, UK) zetasizer instrument with the temperature fixed at 25 °C. The measured hydrodynamic diameters were average values of three measurements.

**$^{19}$F NMR spectroscopy and imaging experiments.** $^{19}$F NMR spectroscopy and imaging experiments were performed on an AMX300 spectrometer interfaced to a 7 T vertical super-wide bore magnet. The system was equipped with a Bruker micro-imaging gradient set and the probe used was a Bruker 5 mm $^{19}$F single-tuned bird-cage resonator probe tuned to 282.404 MHz for fluorine detection. All measurements were performed at ambient temperature.

$^{19}$F spin–spin ($T_2$) relaxation times were measured using the CPMG pulse sequence, which had from 2 to 256 180° pulses in the echo train. A total of 12 data points were collected. The echo times ($\tau$) were separately optimized for each measurement and the values used were between 25 μs and 5 ms. The majority of the data collected could be described by a single exponential function. In some cases, where separate short and long decay rates were clearly present, the curve was better described by the sum of two exponential relaxation decays. Spin–lattice ($T_1$) relaxation times were measured using the standard inversion-recovery pulse sequence, with 16 values of inversion times used. A single $T_1$ relaxation time was observed for all samples. Note that single measurements of $T_1$ and $T_2$ relaxation times were generally performed, although several samples were measured more than once. The repeatability of the measurements was confirmed as better than 15%.

$^{19}$F images were collected using the 3D spin-echo pulse sequence. The field of view was 20 × 20 $mm^2$, and the slice thickness was 2.5 mm in a 128 × 128 × 8 matrix. The echo time was 4.8 ms and the repetition time was three seconds. The results presented here were all acquired by co-adding two acquisitions resulting in a constant imaging time of one hour and 20 minutes.

### Preparation of the aqueous polymer solutions

The statistical copolymers containing quaternized METAI units were dissolved directly in water (salt-free or 0.25 M NaCl). The polymer concentration was either 1 w/v% or 2.5 w/v%. The solutions were stirred for 24 h at ambient temperature. The statistical copolymers containing non-quaternized DMAEMA were not soluble in water without adjustment of the pH. The polymers were dispersed in water (salt-free or 0.25 M NaCl), and HCl was added to obtain the desired pH. The polymer concentration was 1 w/v%. The solutions were stirred for 24 h at ambient temperature.

The block copolymers containing METAI units were dissolved directly in water (salt-free or 0.25 M NaCl). An elevated dissolution temperature of 80 °C was chosen, which is above the glass transition temperature of PTFEMA ($T_{g,PTFEMA}$ = 74 °C, as determined by DSC). The formed nanoparticle solutions were stirred for 3 h at 80 °C and then for 24 h at room temperature. The polymer concentration was either 1 w/v% or 2.5 w/v%. The particle sizes of the nanoparticles were determined by DLS.

The block copolymers containing non-quaternized DMAEMA were not directly soluble in water. The solutions were prepared by first dissolving 20 mg of block copolymer in 2 ml of acetone. Water, 2 ml, was added drop-wise with a syringe pump over the course of 1.5 h, under constant stirring. The formed nanoparticle solutions in 1 : 1 acetone : water were stirred for 24 h, after which they were dialyzed against water for three days to remove the acetone. After dialysis, the concentration of the solutions was adjusted to 1 w/v% by allowing the excess water to evaporate slowly under a slight $N_2$ flow, until only 2 ml of solution were left. The particle sizes of the formed nanoparticles were determined by DLS.

The size of the PTFEMA-*b*-P(TFEMA-DMAEMA) nanoparticles as a function of pH was studied with diluted polymer solutions. The polymer concentration was 0.005 w/v%, and a background NaCl concentration of 0.01 M was used in the solutions. The solutions were prepared by first dissolving 20 mg of block copolymer in 2 ml of acetone. Water, 2 ml, was added drop-wise with a syringe pump over the course of 1.5 h, under constant stirring, to induce the formation of nanoparticles. 16 ml of water were then added quickly to provide a solution of 0.1 w/v% polymeric nanoparticles in 90 : 10 water : acetone mixture. The nanoparticle solutions were stirred for 24 h, after which they were dialyzed against water for three days to remove the acetone. After dialysis, 4 ml of 0.1 M NaCl solution, filtered with 0.25 μm filter, were added. Finally, approximately 15 ml of water were added to obtain a batch solution with 20 mg of polymer in 40 ml of water with 0.01 M NaCl (polymer concentration 0.05 w/v%). From this batch solution, the 0.005 w/v% polymer solutions at different pH values were prepared by diluting with aqueous 0.01 M NaCl solution (filtered with 0.25 μm filters) and by adjusting the pH with drop-wise addition of dilute aqueous solutions of HCl or NaOH. Particle sizes were determined by DLS.

## Results and discussion

### Synthesis of the copolymers

In this study, amphiphilic partly fluorinated polyelectrolytes were synthesized in order to evaluate their potential as $^{19}$F MRI-detectable compounds. The structures of the monomer units are presented in Scheme 2 and the properties of the polymers listed in Table 1. The polymers were either statistical or block copolymers with varying proportions of 2,2,2-trifluoroethyl methacrylate (TFEMA) as the hydrophobic fluorine containing monomer unit and 2-(dimethylamino)ethyl methacrylate (DMAEMA) or its quaternized form [2-(methacryloyloxy)ethyl] trimethyl ammonium iodide (METAI) as the electrostatically charged, cationic monomer unit.

TFEMA was chosen as the fluorine-containing monomer for all the polymers, as it has three equivalent fluorine nuclei, resulting in a single peak of potentially high signal-to-noise ratio (SNR) in the $^{19}$F NMR spectrum, and as it is less hydrophobic than more fluorinated monomer units. DMAEMA and its quaternized form METAI were chosen as the electrostatically charged monomers. DMAEMA is a basic monomer unit, and therefore the degree of cationic charge in the DMAEMA-containing polymers in aqueous solutions was dependent of pH, and increased with decreasing pH. The p$K_a$ value of DMAEMA monomer is 8.4.[28] The average p$K_a$ of PDMAEMA, defined as the pH at which 50% of the DMAEMA units are protonated, is dependent on *e.g.* polymer molecular weight, polymer architecture and the ionic strength of the solution. For multibranched PDMAEMA star polymers in salt-free solutions, average p$K_a$ values as low as 5.9 have been measured.[29] In contrast, METAI monomer unit, which has additional methyl group attached to the DMAEMA amine group by a post-polymerization reaction, is cationically charged independent of pH.

The copolymers were polymerized by transition metal mediated living radical polymerization in toluene with CuBr/*N*-(*n*-pentyl)-2-pyridylmethanimine as catalyst.[30,31] The method provided copolymers with controlled molecular weights and reasonably low molecular weight distributions (Table 1). DMAEMA was used as a hydrophilic monomer in statistical copolymers C-12, C-24 and C-51 and in block copolymers B-20 and B-47. METAI was used in statistical copolymer QC-51, which was a completely quaternized version of C-51 and in block copolymer QB-47, which was a completely quaternized version of B-47.

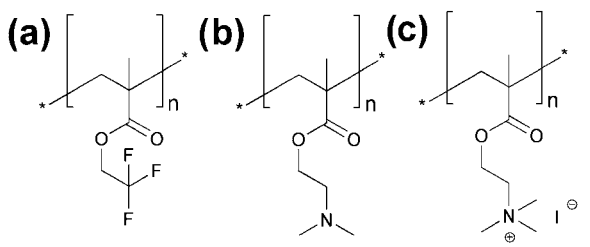


**Scheme 2** The monomers used in the copolymers. (a) 2,2,2-Trifluoroethyl methacrylate (TFEMA), (b) 2-(dimethylamino)ethyl methacrylate (DMAEMA), (c) quaternized DMAEMA, [2-(methacryloyloxy)ethyl] trimethyl ammonium iodide (METAI).

The block copolymers were polymerized in a sequential manner; the TFEMA block was polymerized first and DMAEMA was added when 70–80% TFEMA conversion was reached. Due to the preparation method, the second block was a statistical copolymer, and 20–30% of TFEMA present in the polymer was in the hydrophilic block.

The reactivity ratios of the TFEMA/DMAEMA monomer pair were measured by Jaacks method[27] and they were found to be $r_{TFEMA} = 0.76$ and $r_{DMAEMA} = 0.81$. This indicates that there was no tendency towards formation of blocks within the statistical copolymers or the statistical hydrophilic blocks of the block copolymers. For additional information on the polymerization of the PTFEMA/PDMAEMA copolymers, including polymerization kinetics, calculation of molecular weights from the $^1$H NMR spectra and measurement of reactivity ratios, see ESI†.

### Properties of the aqueous solutions of the copolymers

**Preparation of the solutions.** To evaluate the properties of the synthesized polymers in the aqueous environment, ultimately as components in $^{19}$F MRI-detectable systems, the polymers were dissolved in water (either salt-free or with 0.25 M NaCl). The solutions were characterized using dynamic light scattering, $^{19}$F relaxation time measurements and $^{19}$F imaging experiments.

The polymer concentration in the aqueous solutions was 1 w/v%. The relatively high concentration was chosen to allow the $^{19}$F NMR and $^{19}$F MRI measurements. The statistical copolymers were dissolved directly in water. The block copolymers were assembled into aqueous nanoparticles, either through solvent exchange from acetone, or by direct dissolution at elevated temperature. In order to study the effect of solution conditions on the $^{19}$F NMR performance of the polymers, the non-quaternized statistical copolymers were studied at varying pH and salt conditions.

Details of the polymer solutions are presented in Table 2, along with the results of the measurements performed with the solutions. In addition, estimations of the polymer conformations (collapsed or extended), based on the combined measurement results, are presented in Table 2 for each polymer solution. However, these conformation estimations represent only relative qualities between the samples, and do not indicate the absolute extent of the collapse or extension of the chains.

**Dynamic light scattering (DLS) measurements.** The block copolymers were expected to form nanoparticles in aqueous solutions. Particle size of the block copolymer solutions was studied by DLS. The results show (Table 2) that the non-quaternized block copolymers B-20 and B-47, which were dissolved in salt-free water *via* solvent exchange from acetone, formed particles with hydrodynamic diameters ($D_H$) of 45 nm and 29 nm, respectively. The quaternized block copolymer QB-47, which was directly dissolved in water with 0.1 M NaCl at elevated temperature, had a broad size distribution in the DLS curve. It is possible that the dissolution of QB-47 was not ideal under the chosen conditions.

In addition to the solution experiments described in Table 2, a set of DLS experiments were conducted, where the hydrodynamic diameters of B-47 nanoparticles were studied as a function of pH. However, these experiments were conducted with more

**Table 1** Properties of the polymer samples. The samples are named according to their molar TFEMA content

| Sample | Composition | TFEMA content (mol%) | F content/mmol $g^{-1}$ | $M_n$[a]/g $mol^{-1}$ (NMR) | $M_w/M_n$[b] |
|---|---|---|---|---|---|
| Statistical copolymers | | | | | |
| C-12 | P($TFEMA_{17}$-*co*-$DMAEMA_{122}$) | 12 | 2.3 | 22 000 | 1.39 |
| C-24 | P($TFEMA_{34}$-*co*-$DMAEMA_{109}$) | 24 | 4.5 | 22 900 | 1.39 |
| C-51 | P($TFEMA_{75}$-*co*-$DMAEMA_{73}$) | 51 | 9.3 | 24 100 | 1.24 |
| QC-51 | P($TFEMA_{75}$-*co*-$METAI_{73}$) | 51 | 6.6 | 34 400 | 1.24[c] |
| Block copolymers | | | | | |
| B-20 | $PTFEMA_{39}$-*b*-P($DMAEMA_{197}$-*co*-$TFEMA_{12}$) | 20 | 3.8 | 39 500 | 1.55 |
| B-47 | $PTFEMA_{91}$-*b*-P($DMAEMA_{122}$-*co*-$TFEMA_{19}$) | 47 | 8.9 | 37 700 | 1.43 |
| QB-47 | $PTFEMA_{91}$-*b*-P($METAI_{122}$-*co*-$TFEMA_{19}$) | 47 | 6.1 | 55 000 | 1.43[c] |

[a] Calculated from $^1$H NMR spectra by comparing end-group peaks to appropriate side-chain peaks. [b] By SEC with DRI detection. [c] Measured before quaternization.

dilute, 0.005 w/v% nanoparticle solutions, and also the nanoparticle preparation conditions were slightly different from those applied in Table 2. Therefore, the results are expected to give only a qualitative estimation on how the B-47 particles described in Table 2 behave if the pH is altered. The hydrodynamic diameters of the B-47 particles obtained at varying pH conditions are shown in Table 3.

The results in Table 3 show that the $D_H$ of the particles approximately doubled when the pH was lowered from 9 to 3.

The corona blocks of the particles consisted of a statistical copolymer of TFEMA and DMAEMA containing 13 mol% of TFEMA units (Table 1). The blocks had low charge density at pH 9 whereas they had high charge density at pH 3.

Since the particles had highly hydrophobic cores which were below the glass transition temperature ($T_{g,TFEMA}$ = 74 °C as measured by differential scanning calorimetry) they were expected to be kinetically trapped structures.[32,33] Therefore the change in $D_H$ is not expected to derive from changes in the aggregation number, as the pH adjustment was done as the final step, after the particles were formed. Alternatively, the change in the $D_H$ must derive from the significant expansion of the corona chains with increasing charge density, as suggested in Scheme 1. Based on these results it can be expected that qualitatively similar expansion with increasing charge density could also take place in the particles of the other block copolymer samples, as well as in the statistical copolymer coils. Similar responsiveness to changes in pH has been visualized for PDMAEMA in an AFM study of PDMAEMA cylindrical brushes.[15]

**$^{19}$F NMR and $^{19}$F MRI: relaxation time studies and imaging of the polymer solutions.** The spin–lattice ($T_1$) and spin–spin ($T_2$) relaxation times of the $^{19}$F nuclei along with the $^{19}$F image intensities of phantom images were measured of the prepared polymer solutions in order to evaluate the applicability of the

**Table 2** Properties of the aqueous polymer solutions. Solution conditions, nanoparticle hydrodynamic diameters by DLS (only for block copolymers), $^{19}$F NMR relaxation times, SNR of $^{19}$F MRI images and expected solution conformations of the copolymers. Polymer concentration was 1 w/v% in the solutions. Non-quaternized statistical copolymers were studied at varying pH conditions and salt concentrations, for the other samples only one set of solution conditions were applied

| | Solution conditions | | | | | | |
|---|---|---|---|---|---|---|---|
| Sample | pH | [NaCl]/M | $D_H$/nm (DLS) | $^{19}$F $T_1$/ms | $^{19}$F $T_2$/ms | SNR in $^{19}$F MRI | Expected conformation of the copolymer in solution |
| Statistical non-quaternized copolymers, with varying solution pH and ionic strength | | | | | | | |
| C-12 | 8 | 0 | | 320 | 13 | No signal | Collapsed globule |
| | 8 | 0.25 | | 310 | 12 | —[a] | Collapsed globule |
| | 6.5 | 0 | | 520 | 140 | 3.9 | Extended coil |
| | 7.3 | 0.25 | | 460 | 76 | —[a] | Extended (intermediate) coil |
| | 2 | 0 | | 550 | 140 | 3.9 | Extended coil |
| | 2 | 0.25 | | 520 | 160 | —[a] | Extended coil |
| C-24 | 6.5 | 0 | | 430 | 81 | 6.0 | Extended (intermediate) coil |
| | 2 | 0 | | 540 | 150 | 6.2 | Extended coil |
| | 2 | 0.25 | | 490 | 120 | —[a] | Extended coil |
| C-51 | 2 | 0 | | 360 | 11 | 6.9/(14)[b] | Collapsed globule |
| | 2 | 0.25 | | 320 | 8.4 | 5.5 | Collapsed globule |
| Other samples | | | | | | | |
| QC-51 | | 0.25 | | 330 | 11 | Weak signal/(9.2)[b] | Collapsed globule |
| B-20[c] | | 0 | 45[d] | 340 | 69% 0.12 31% 11 | No signal | Collapsed nanoparticle |
| B-47[c] | | 0 | 29[d] | 400 | 86% 0.22 14% 11 | No signal | Collapsed nanoparticle |
| QB-47[e] | | 0.25 | 20–1000[f] | 480[g] | 89% 0.73 11% 81[g] | No signal/(3.4)[b] | Extended nanoparticle |

[a] Not measured. [b] The result in parentheses is for more concentrated, 2.5 w/v% solution. [c] Dissolved by solvent exchange from acetone. [d] Relative standard deviation was <2%. [e] Dissolved at elevated temperature (80 °C). [f] A broad size distribution was obtained, the extreme values are reported. The DLS measurement was done in 0.1 M NaCl. [g] Measured with 2.5 w/v% solution.

**Table 3** Hydrodynamic diameter of B-47 particles at different pH conditions, as measured by DLS. Polymer concentration was 0.005 w/v% and the solutions contained 0.01 M NaCl

| pH | $D_H$/nm (DLS) |
|---|---|
| 3 | 80[a] |
| 6.5 | 50[a] |
| 9 | 41[a] |

[a] Relative standard deviation < 5%.

samples for $^{19}$F MRI. For a spin-echo imaging sequence, the image intensity is expected to be proportional to the NMR parameters as described in eqn (1).[34]

$$I \approx N(\mathrm{F}) \times \left[1 - 2\exp\left(\frac{1(T_R - T_E/2)}{T_1}\right) + \exp\left(\frac{-T_R}{T_1}\right)\right]\exp\left(\frac{-T_E}{T_2}\right) \quad (1)$$

In eqn (1) $I$ is the image intensity, $N$(F) a measure of the number of fluorine nuclei in the sensitive volume of the imager, $T_R$ and $T_E$ are the pulse sequence repetition and echo times, respectively.

Eqn (1) states that the most effective imaging agents will have short $T_1$ relaxation times, long $T_2$ relaxation times and high fluorine contents. Both $T_1$ and $T_2$ are affected by the mobility of the nuclei in question, in this case fluorine. The relaxation time results of the solutions are presented in Table 2 and the fluorine contents of the polymers are presented in Table 1.

The SNR of the phantom $^{19}$F images, describing the image intensity, is also presented in Table 2. The images were taken with a spin-echo imaging sequence, where the echo time was 4.8 ms and the repetition time was 3 s. The imaging time was restricted to 80 min. For some samples the polymer concentration in the solutions was increased from the 1 w/v% used in the relaxation measurements to 2.5 w/v% in order to get images of higher SNR. The SNR results of these more concentrated solutions are presented in parentheses in Table 2.

As a preliminary overview of the $^{19}$F NMR and $^{19}$F MRI results in Table 2 it can be seen that differences in both relaxation rates were observed with changes in the polymer structures and solution conditions. The values of $T_1$ ranged from 310 ms to 550 ms. However, more significant differences in the values of $T_2$ were observed between the samples, where variation greater than two orders of magnitude was observed: from values less than 1 ms to 160 ms. The relatively small variation between $T_1$ values indicates that the spectral density of motion of the fluorine nuclei in the mid-MHz range was not highly affected by conformational differences, although systematically the $T_1$ relaxation times of the collapsed structures were lower than those observed for the extended structures. The $T_2$ relaxation times, which are sensitive to lower frequency motions, were much more sensitive to changes in conformation.

The observed differences in the relaxation times, along with varying fluorine contents, resulted in different SNR in $^{19}$F MRI. In particular the $T_2$ relaxation times were found to be highly indicative of the sample performance, and the $T_2$ results are therefore discussed with special attention in the following sections. The detailed $T_2$ results, including the exponential fitting of the data, are presented in ESI†.

**$^{19}$F NMR and $^{19}$F MRI results: statistical copolymers.** The non-quaternized statistical copolymers C-12, C-24 and C-51 were studied at several solution conditions; at varying pH values and either in salt-free or in 0.25 M NaCl solutions. Even though such changes in solution conditions are not applicable *in vivo*, the results are useful as they give information on how the polymer conformation in aqueous solution affects the $^{19}$F relaxation times and subsequently the $^{19}$F MRI intensities. The quaternized statistical copolymer QC-51 was studied only at one set of conditions; with unadjusted pH and 0.25 M NaCl. In general, changes in pH had a significantly larger effect on relaxation times than changes in salt concentration, as seen in Table 2. Therefore, it is possible to examine the effect of pH by considering only the results for the 0.25 M NaCl solutions, as the relaxation time results from salt-free solutions were in most cases similar.

Sample C-12 contained only 12 mol% TFEMA, and was soluble in water even at pH 8, where the extent of DMAEMA protonation was low. At this pH both relaxation rates of $^{19}$F were relatively short, $T_1$ = 310 ms and $T_2$ = 12 ms (0.25 M NaCl solution, Table 2). When the pH was decreased, the relaxation rates increased substantially, especially $T_2$, which at pH 2 increased one order of magnitude to $T_2$ = 160 ms (0.25 M NaCl solution). This change is expected to be due to a globule-to-coil transformation in the chain conformation, as drawn in Scheme 1 and tabulated in Table 2. When the pH was decreased, the repulsion between cationic monomer units increased, overcoming the attraction between the hydrophobic –$CF_3$ and –$CH_3$ groups in the copolymer. This resulted in increased segmental mobility around the –$CF_3$ groups, which increased the $^{19}$F $T_2$ relaxation time.

C-24, which contained 24 mol% of TFEMA, was no longer soluble in water at pH 8. Otherwise, the behavior of the sample as a function of pH was similar to C-12. Most notably at pH 2, when the extent of DMAEMA protonation was high, the relaxation results of C-24 and C-12 were similar, *e.g.* at 0.25 M NaCl solutions $T_2$ of C-12 and C-24 were 160 ms and 120 ms, respectively (Table 2). C-51, which contained 51 mol% of TFEMA groups was not soluble in water even at pH 6.5, and was measured only at pH 2. The relaxation rates of C-51 at pH 2 were significantly decreased from the other two samples at low pH, down to values $T_1$ = 320 ms and $T_2$ = 8.4 ms (0.25 M NaCl solution), similar to the collapsed form of C-12 at pH 8. This indicates that at this highest fluorine content, the electrostatic repulsion was not sufficiently strong to overcome the attraction between the numerous –$CF_3$ groups in the copolymer chain. These trends in the aqueous conformations of hydrophobic polyelectrolytes have been predicted theoretically.[13] The quaternized sample QC-51 was soluble in water without adjustment of pH. The relaxation times measured for QC-51 were very close to values measured for C-51 at pH 2, which is not surprising, as both samples had equal charge and TFEMA densities.

When comparing the relaxation rate results of salt-free and 0.25 M NaCl solutions, it can be seen from Table 2 that the $T_2$ relaxation time of C-12 at pH 6.5 in salt-free solution ($T_2$ = 140 ms) is almost twice as large as the corresponding $T_2$ of C-12 at pH 7.3 in 0.25 M NaCl solution ($T_2$ = 76 ms). However, in

 

general it is difficult to draw conclusions from the differences between these two samples as it is difficult to estimate the charge density of the polymers. The samples were in the pH range where relatively significant HCl additions resulted in minor changes in the solution pH, but in major changes in the charge density of the polymer. This area often appears in the titration curves of hydrophobic polyelectrolytes before the neutralization point, and has been argued to derive from the phase transition between the collapsed and extended states.[13]

The reason for the different pH values in the intermediate pH C-12 samples (6.5 for salt-free solution and 7.3 for 0.25 M NaCl solution) was that both the solutions were prepared with approximately equal amounts of added HCl. DMAEMA units were more readily protonated in 0.25 M NaCl solutions than in salt-free solutions, due to the screening of the polymer chain charges by the salt.

Otherwise, if the pH values 6.5–7.3 were not taken into consideration, the comparison of relaxation rate results of salt-free and 0.25 M NaCl solutions revealed only small differences. The general trend was that in most cases the salt-free solutions had slightly longer relaxation times, but the differences were not large. In theory, increasing the ionic strength of the solution should have a significant impact on the solution conformation of hydrophobic polyelectrolytes.[11,13,17,18] However, due to the high polymer concentration of the solutions, the ionic strength of the salt-free solutions was already rather high. This could explain why no differences in the relaxation rates were observed between the salt free and 0.25 M NaCl solutions.

When comparing these relaxation rate results to the performance of the samples in imaging experiments, it can be seen that increasing $T_2$ indeed increased the image intensity, as suggested by eqn (1). C-12 could not be imaged at pH 8 ($T_2 = 13$ ms, salt-free solution) but at pH 2 ($T_2 = 140$ ms, salt-free solution) it gave a weak image (SNR = 3.9). However, the samples C-24 and C-51 at pH 2 resulted in roughly equal image intensities. The one-magnitude shorter $T_2$ of C-51 ($T_2 = 8.4$ ms, salt-free solution) when compared to C-24 ($T_2 = 150$ ms, salt-free solution) was completely compensated by the increase in the fluorine nuclei present in the polymer chain. The samples C-51 at pH 2 and QC-51 had approximately equal relaxation times. The higher intensity of the C-51 image most likely resulted from the higher fluorine content of the sample (Table 1); the fluorine content of the quaternized QC-51 was significantly reduced by the incorporation of heavy iodine ions into METAI units.

In summary, there was a clear balance in behaviour: increasing fluorine content on one hand increased the image intensity by adding more $^{19}$F nuclei to the image, but on the other hand decreased the $T_2$ relaxation time, potentially reducing the image intensity, because of increased association between the more abundant fluorinated groups. From the results of the C-12, C-24, C-51 and QC-51 series it can be concluded that optimal images would be obtained if extended coil conformation could be retained at high fluorine contents. On the other hand, it can be seen that if the $T_2$ remains at a reasonably high level, as in C-51 at pH 2 and in QC-51, images can be obtained even if mobility is restricted to some extent.

**$^{19}$F NMR and $^{19}$F MRI results: block copolymer nanoparticles.** The block copolymer samples were successfully assembled to nanoparticles in aqueous solutions, as shown by the DLS results (Table 2). The expected solution structure for the block copolymers was a particle, where the hydrophobic PTFEMA block formed the core and the statistical PTFEMA/PDMAEMA copolymer formed the corona (Scheme 1). PTFEMA has a relatively high glass transition temperature, 74 °C (DSC), and therefore the cores of the particles were expected to be rather rigid and have short $T_2$ values. On the other had, the TFEMA units present in the corona blocks were expected to have more mobility.

Large variations were again observed in the $T_2$ relaxation rates. Two different $T_2$ values could be separated from the $T_2$ relaxation curves of all the nanoparticle solutions (Table 2, for the relaxation decays see ESI†). The presence of two separate $T_2$ values indicates the presence of separate $^{19}$F populations, at least on the time scale of the relaxation time measurements. It can be assumed that the shorter $T_2$ derives from the TFEMA units within the core blocks of the particles, while the longer $T_2$ is due to the TFEMA units within the statistical copolymer blocks forming the coronas of the particles. The relative populations of short and long $^{19}$F $T_2$ values could be estimated from the relaxation decays (listed in Table 2) and correspond to the relative TFEMA populations in the core and corona blocks reasonably well. For example the B-47 block copolymer had 17% of its TFEMA groups in the statistical corona block, and correspondingly the relative size of the $^{19}$F population with long $T_2$ was measured to be 14%.

The major component in the $T_2$ relaxation times of the block copolymer particles was short, <1 ms relaxation time arising from the particle cores. These values were so short that in practice the core $^{19}$F nuclei did not contribute to the MRI images with the pulse sequence we used (with echo time of 4.8 ms). Thus, only the nuclei present within the corona blocks were detected in the images.

The corona blocks of the block copolymer samples were statistical copolymers, and their $^{19}$F NMR properties were found to follow similar trends as the statistical copolymers discussed above. The TFEMA unit density of the corona blocks was either 6 mol% (B-20) or 13 mol% (B-47 and QB-47). The environment for the fluorine atoms in the coronas of the B-20 and B-47 particles was therefore similar to the environment for fluorine in C-12 chains at pH 8 as the chain charge densities were in all cases low (the block copolymers were measured at unadjusted pH) and the fluorine contents similar. Correspondingly, the environment for fluorine in the coronas of QB-47 particles was similar to the environment for fluorine in C-12 chains at pH 2, because the charge densities were now high in both cases, and the fluorine contents again similar.

The long $T_2$ component of both B-20 and B-47 was $T_2 = 11$ ms, which was almost the same as the value measured for C-12 at pH 8, $T_2 = 13$ ms (0 M NaCl in both measurements, Table 2). The long $T_2$ component of QB-47 was $T_2 = 81$ ms. This was somewhat lower than the value for the C-12 at pH 2, $T_2 = 140$ ms (0 M NaCl in both measurements, Table 2). However, the trend of increasing $T_2$ relaxation time with increasing charge density was evident both in the case of block copolymer coronas and in the case of statistical copolymers.

The similarities in the results of the C-12 statistical copolymers with the corresponding corona blocks of the nanoparticles

indicate that the results we obtained with statistical copolymers can be used to qualitatively estimate the behavior of corresponding nanoparticle coronas. However, the systems are not exactly comparable due to the extra confinement effects provided by the particle cores.

The DLS results for the B-47 particles as a function of solution pH (Table 3) indicated that the conformation of the block copolymer particle coronas was highly dependent on the charge density of the corona block. The relaxation time results in Table 2 strongly support this conclusion. The conformations of the B-20 and B-47 particles are therefore expected to be compact (low charge density, short $T_2$) whereas the conformation of the QB-47 particles is expected to be extended (high charge density, long $T_2$), as depicted in Scheme 1 and tabulated in Table 2. The DLS measurements in Table 3 gave indication only of the behavior of the block copolymers, but since the relaxation rates followed similar trends in both the block copolymer and statistical copolymer samples, it can be expected that such collapse and extension phenomena were present in the statistical copolymers as well.

None of the nanoparticle solutions gave distinguishable MRI signals at 1 w/v% concentration. When the QB-47 sample was concentrated to 2.5 w/v% concentration, a weak image was obtained. However, the weaker imaging performance of the nanoparticle solutions when compared to statistical copolymers is understandable—because the core block formed the majority of the block copolymer chains, the concentration of the detectable corona fluorine nuclei was low in the nanoparticle solutions. Nanoparticles constructed from such block copolymers, where the corona block forms the majority of the chain, are expected to perform significantly better in $^{19}$F MRI, if the overall concentration is kept constant.

## Conclusions

A series of partly fluorinated, electrostatically charged statistical and block copolymers were synthesized and studied in aqueous solutions. The aim of the study was to evaluate the performance of the polyelectrolytes in $^{19}$F MRI, especially as corona components in $^{19}$F-detectable nanoparticles. The copolymers had TFEMA as fluorine-containing monomer unit copolymerized with cationic DMAEMA or METAI units. It was noticed that maintaining sufficient mobility of the $^{19}$F nuclei was important for obtaining images of high intensity. Mobility of the fluorinated groups could be increased by preventing their aggregation in water by exploiting electrostatic repulsion between monomer units. The $^{19}$F NMR $T_2$ relaxation times were found to be highly indicative of the sample $^{19}$F imaging performance. Conversely, it was noticed that if sufficient $^{19}$F mobility was achieved having a high fluorine density in the polymer was important to obtain an image of high intensity. Block copolymers assembled into nanoparticles were found to perform in the $^{19}$F NMR experiments in a similar manner to statistical copolymers, provided that the fluorine groups remained within the particle coronas. The imaging performance of the fluorinated rigid particle cores, consisted of PTFEMA homopolymer, was poor.

In order to achieve superior imaging performance it is necessary to retain the fluorine group mobility with higher fluorine loadings. If the $^{19}$F nuclei are incorporated in the coronas of the nanoparticles, as in this study, one solution could be to increase the hydrophilicity of the corona blocks, and especially incorporate hydrophilic functionalities as close to the $^{19}$F nuclei as possible. Another way of achieving high $^{19}$F detectability could be the synthesis of nanoparticles with liquid-like fluorophilic cores, where large amounts of fluorinated compounds could be incorporated.

## Acknowledgements

The authors acknowledge financial support from the Graduate School in Chemical Engineering (Finland). Financial support from the Queensland Government for funding under the NIRAP scheme for the International Biomaterials Research Alliance is also gratefully acknowledged. Part of this work utilized equipment funded under the NCRIS Australian National Fabrication Facility.

## Notes and references

1 J. Yu, V. D. Kodibagkar, W. Cui and R. P. Mason, *Curr. Med. Chem.*, 2005, **12**, 819–848.
2 J. M. Janjic, M. Srinivas, D. K. K. Kadayakkara and E. T. Ahrens, *J. Am. Chem. Soc.*, 2008, **130**, 2832–2841.
3 W. Du, A. M. Nyström, L. Zhang, K. T. Powell, Y. Li, C. Cheng, S. A. Wickline and K. L. Wooley, *Biomacromolecules*, 2008, **9**, 2826–2833.
4 W. Du, Z. Xu, A. M. Nyström, K. Zhang, J. R. Leonard and K. L. Wooley, *Bioconjugate Chem.*, 2008, **19**, 2492–2498.
5 H. Peng, I. Blakey, B. Dargaville, F. Rasoul, S. Rose and A. K. Whittaker, *Biomacromolecules*, 2009, **10**, 374–381.
6 A. M. Nyström, J. W. Bartels, W. Du and K. L. Wooley, *J. Polym. Sci., Part A: Polym. Chem.*, 2009, **47**, 1023–1037.
7 J. M. Criscione, B. L. Le, E. Stern, M. Brennan, C. Rahner, X. Papademetris and T. M. Fahmy, *Biomaterials*, 2009, **30**, 3946–3955.
8 M. Higuchi, N. Iwata, Y. Matsuba, K. Sato, K. Sasamoto and T. C. Saido, *Nat. Neurosci.*, 2005, **8**, 527–533.
9 P. Mirau, *Practical Guide to Understanding the NMR of Polymers*, John Wiley & Sons, Inc., Hoboken, New Jersey, 2005.
10 A. V. Dobrynin, *Curr. Opin. Colloid Interface Sci.*, 2008, **13**, 376–388.
11 A. V. Dobrynin and M. Rubinstein, *Prog. Polym. Sci.*, 2005, **30**, 1049–1118.
12 J. Kötz, S. Kosmella and T. Beitz, *Prog. Polym. Sci.*, 2001, **26**, 1199–1232.
13 S. Ulrich, A. Laguecir and S. Stoll, *J. Chem. Phys.*, 2005, **122**, 094911.
14 O. V. Borisov, F. Hakem, T. A. Vilgis, J. F. Joanny and A. Johner, *Eur. Phys. J. E*, 2001, **6**, 37–47.
15 Y. Xu, S. Bolisetty, M. Drechsler, B. Fang, J. Yuan, M. Ballauff and A. H. E. Müller, *Polymer*, 2008, **49**, 3957–3964.
16 L. J. Kirwan, G. Papastavrou, M. Borkovec and S. H. Behrens, *Nano Lett.*, 2004, **4**, 149–152.
17 S. Minko, A. Kiriy, G. Gorodyska and M. Stamm, *J. Am. Chem. Soc.*, 2002, **124**, 3218–3219.
18 A. Kiriy, G. Gorodyska, S. Minko, W. Jaeger, P. Stepanek and M. Stamm, *J. Am. Chem. Soc.*, 2002, **124**, 13454–13462.
19 J. Preuschen, S. Menchen, M. A. Winnik, A. Heuer and H. W. Spiess, *Macromolecules*, 1999, **32**, 2690–2695.
20 I. Furo, I. Iliopoulos and P. Stilbs, *J. Phys. Chem. B*, 2000, **104**, 485–494.
21 G. D. Poe, W. L. Jarrett, C. W. Scales and C. L. McCormick, *Macromolecules*, 2004, **37**, 2603–2612.
22 A. J. Convertine, B. S. Lokitz, Y. Vasileva, L. J. Myrick, C. W. Scales, A. B. Lowe and C. L. McCormick, *Macromolecules*, 2006, **39**, 1724–1730.
23 J. Pietrasik, B. S. Sumerlin, H. Lee, R. R. Gil and K. Matyjaszewski, *Polymer*, 2007, **48**, 496–501.
24 R. N. Keller and H. D. Wycoff, *Inorg. Synth.*, 1946, **2**, 1–4.
25 D. M. Haddleton, C. B. Jasieczek, M. J. Hannon and A. J. Shooter, *Macromolecules*, 1997, **30**, 2190–2193.

 

26 N. J. Hovestad, G. van Koten, S. A. F. Bon and D. M. Haddleton, *Macromolecules*, 2000, **33**, 4048–4052.
27 V. Jaacks, *Makromol. Chem.*, 1972, **161**, 161–172.
28 P. van de Wetering, N. J. Zuidam, M. J. van Steenbergen, O. A. G. J. van der Houwen, W. J. M. Underberg and W. E. Hennink, *Macromolecules*, 1998, **31**, 8063–8068.
29 F. A. Plamper, M. Ruppel, A. Schmalz, O. Borisov, M. Ballauff and A. H. E. Muller, *Macromolecules*, 2007, **40**, 8361–8366.
30 N. M. L. Hansen, K. Jankova and S. Hvilsted, *Eur. Polym. J.*, 2007, **43**, 255–293.
31 N. M. L. Hansen, M. Gerstenberg, D. M. Haddleton and S. Hvilsted, *J. Polym. Sci., Part A: Polym. Chem.*, 2008, **46**, 8097–8111.
32 G. Riess, *Prog. Polym. Sci.*, 2003, **28**, 1107–1170.
33 O. Théodoly, M. Jacquin, P. Muller and S. Chhun, *Langmuir*, 2009, **25**, 781–793.
34 R. E. Hendrick, *Magn. Reson. Imaging*, 1987, **5**, 31–37.

Supplementary Material (ESI) for Polymer Chemistry


**Electronic Supplementary Information**

# Synthesis and evaluation of partly-fluorinated polyelectrolytes as components in $^{19}$F MRI-detectable nanoparticles

Leena Nurmi, Hui Peng, Jukka Seppälä, David M. Haddleton, Idriss Blakey and Andrew K. Whittaker*

* Correspondence to: Andrew Whittaker, E-mail: a.whittaker@uq.edu.au

Contents:



**Experimental details for the synthesis of block copolymers of TFEMA and DMAEMA.** The polymerizations were conducted with a [DMAEMA]+[TFEMA]:[CuBr]:[ligand]:[initiator] ratio of 150:1:2.2:1 and monomer/solvent ratio of 1:1 (v:v). The block copolymers were prepared by one-pot sequential polymerization, where PTFEMA block was prepared first and DMAEMA monomer was added at around 80% TFEMA conversion.

Typically: TFEMA (1.6 ml, 11 mmol), *N*-(*n*-pentyl)-2-pyridylmethanimine (119 mg, 0.68 mmol), benzyl 2-bromoisobutyrate (79 mg, 0.31 mmol) and toluene (7.4 ml) were added to a small Schlenk tube. The solution was deoxygenated by three freeze-pump-thaw cycles. Into another small Schlenk tube, CuBr (44 mg, 0.31 mmol) was added, and the tube was evacuated and back-filled with nitrogen several times. The toluene solution was cannulated into this tube. The tube was immersed into a pre-heated, thermostated oil bath at 90 °C. During polymerization, samples were withdrawn at certain time

intervals (with cannula, under $N_2$ flow) from the polymerization mixture to follow the development of conversion (by $^1$H NMR in *d*-chloroform).

At around 80 % TFEMA conversion, deoxygenated DMAEMA (5.8 ml, 35 mmol) was added. The polymerization was stopped when around 70-80% DMAEMA conversion was reached. The polymerization mixture was diluted with toluene and purged with air overnight. The mixture was passed through basic alumina to remove the catalyst. The product was precipitated from cold petroleum ether several times.

The block copolymers were purified by removal of traces of PTFEMA homopolymer by acidification of a solution of the crude polymer in THF with diluted HCl (aq), which led to the exclusive precipitation of the PTFEMA/PDMAEMA block copolymer. The precipitated polymer was recovered by centrifugation, and dissolved in 90:10 THF/triethylamine mixture. The formed salt was removed by filtration and the polymer was precipitated from cold petroleum ether. The purification was followed by SEC (in THF/triethylamine 95:5 v:v , with UV detection at 250 nm). If necessary, the purification was repeated.

**Experimental details for the synthesis of statistical copolymers of TFEMA and DMAEMA.** The statistical copolymers were polymerized with otherwise similar conditions as the block copolymers, but DMAEMA was added to the mixture at the beginning of the polymerization. Statistical copolymers C-12 and C-24 were polymerized at 90 ºC and C-51 was polymerized at 60 ºC.

**Polymerization results for TFEMA-DMAEMA block and statistical copolymers.** *Polymerization kinetics*. The kinetic curves measured by $^1$H NMR (in *d*-chloroform) for the block copolymerizations are presented in Figure 1 and for the statistical copolymerizations in Figure 2. The kinetic curves were linear up to high conversions. The curves were calculated by comparing the relative intensities of the monomer peaks (TFEMA 1H at 6.21 ppm, 1H at 5.67 ppm, 2H at 4.50 ppm; DMAEMA 1H at 6.11 ppm, 1H at 5.55 ppm, 2H at 4.24 ppm) to the relative intensities of the polymer side-chain peaks (PTFEMA 2H at 4.33 ppm, PDMAEMA 2H at 4.07 ppm).

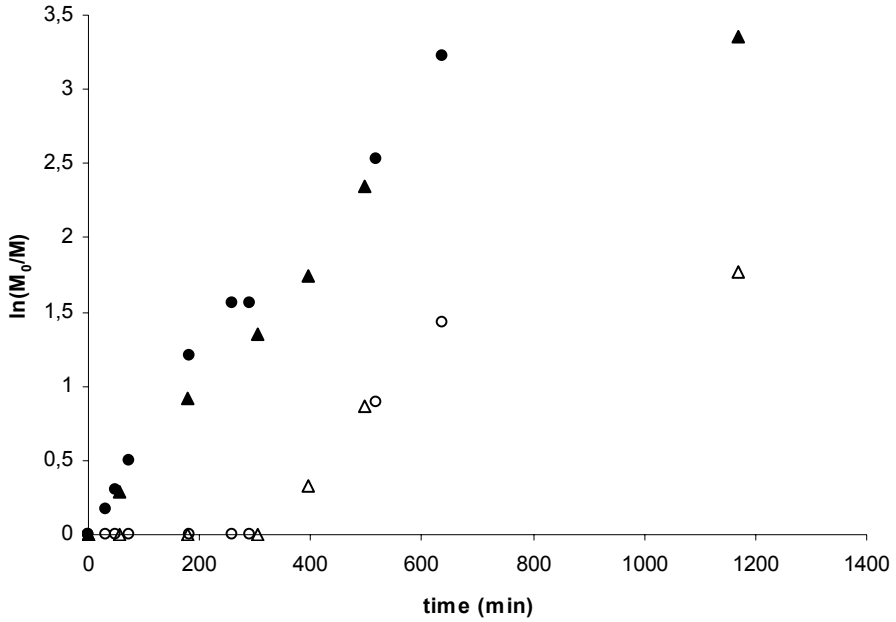


Figure 1. Kinetic curves for the block copolymerizations. ▲ B-20, TFEMA. Δ B-20, DMAEMA. ● B-47, TFEMA. ○ B-47, DMAEMA. For both polymerizations, DMAEMA was added 300 min after the reaction was started.

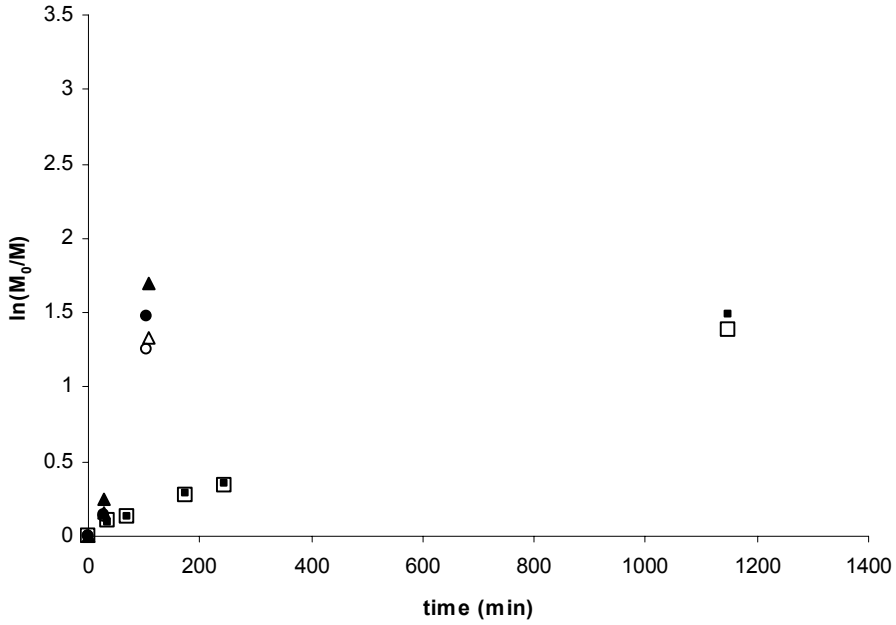

Figure 2. Kinetic curves for the statistical copolymerizations. ▲ C-12, TFEMA. Δ C-12, DMAEMA. ● C-24, TFEMA. ○ C-24, DMAEMA. ■ C-51, TFEMA. □ C-51, DMAEMA. The polymers C-12 and C-24 were polymerized at 90 °C, the polymer C-51 was polymerized at 60 °C.

*Molecular weights.* The molecular weights of the copolymers were calculated from the $^1$H NMR spectra (in *d*-chloroform) of the purified copolymers, by comparing the end-group peaks deriving from the initiator (2H at 5.07 ppm and 5H at 7.34 ppm) to appropriate side-chain peaks. The molecular weights calculated from the $^1$H NMR spectra were always higher than theoretical molecular weights (Table 1). This is expected to derive from incomplete initiator efficiency and for block copolymers also from partial termination of the first block when the polymerization of the second block was started. The PTFEMA homopolymer was removed from the block copolymer samples, which increased their average molecular weights. The purification step in the block copolymer synthesis may also have removed block copolymers with smallest molecular weights from the samples, further increasing their molecular weights.

Table 1. Theoretical and experimental molecular weights of the PTFEMA/PDMAEMA copolymers.

| Sample | Theoretical $M_n$[a] (g/mol) | Experimental $M_n$ (by $^1$H NMR) (g/mol) |
|---|---|---|
| C-12 | 17200 | 22000 |
| C-24 | 17400 | 22900 |
| C-51 | 18600 | 24100 |
| B-20 | 20800 | 39500 |
| B-47 | 21100 | 37700 |

[a] calculated for the monomer conversions, at which the polymerizations were stopped.

**Reactivity ratio measurements of the TFEMA/DMAEMA monomer pair.** The reactivity ratios of the TFEMA/DMAEMA pair were measured with the Jaacks method [1-3]. The method involves the use of a large excess of one monomer ($M_1$) relative to the other one ($M_2$). The reactivity ratio of the monomer in excess is obtained from the linear logarithmic plot of monomer conversions:

$$r_1 = \frac{\ln \frac{[M_1]_0}{[M_1]}}{\ln \frac{[M_2]_0}{[M_2]}} \qquad (1)$$

where $[M_i]_0$ and $[M_i]$ are the initial concentration of monomer i and the concentration of unreacted monomer i after a given polymerization time, respectively.

The Jaacks plots were generated from TFEMA/DMAEMA copolymerizations at 95:5 and 5:95 molar ratios. The polymerizations were conducted with CuBr/*N*-(*n*-pentyl)-2-pyridylmethanimine catalyst system, and toluene as solvent (1:1 v7v) at 90 °C (same conditions as in the other statistical copolymerizations of TFEMA and DMAEMA). The plots are presented in Figure 3 and Figure 4. From the plots, the reactivity ratios measured for the TFEMA/DMAEMA monomer pair were $r_{TFEMA} = 0.76$ and $r_{DMAEMA} = 0.81$. The values correspond to a rather random copolymerization with no tendency towards formation of blocks within the polymer chain.

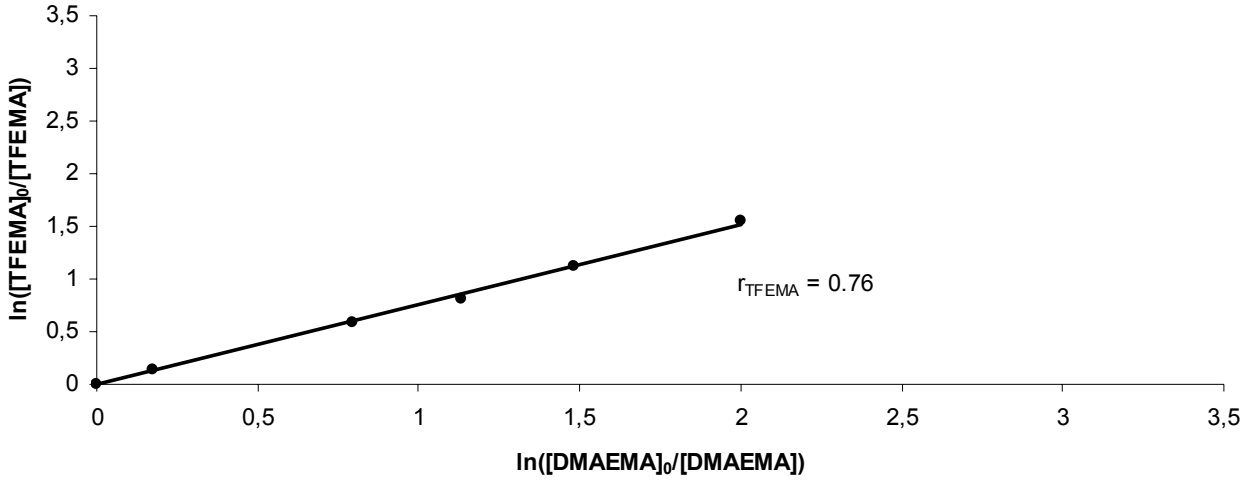


Figure 3. Jaacks plot of the copolymerization of TFEMA and DMAEMA (95:5).

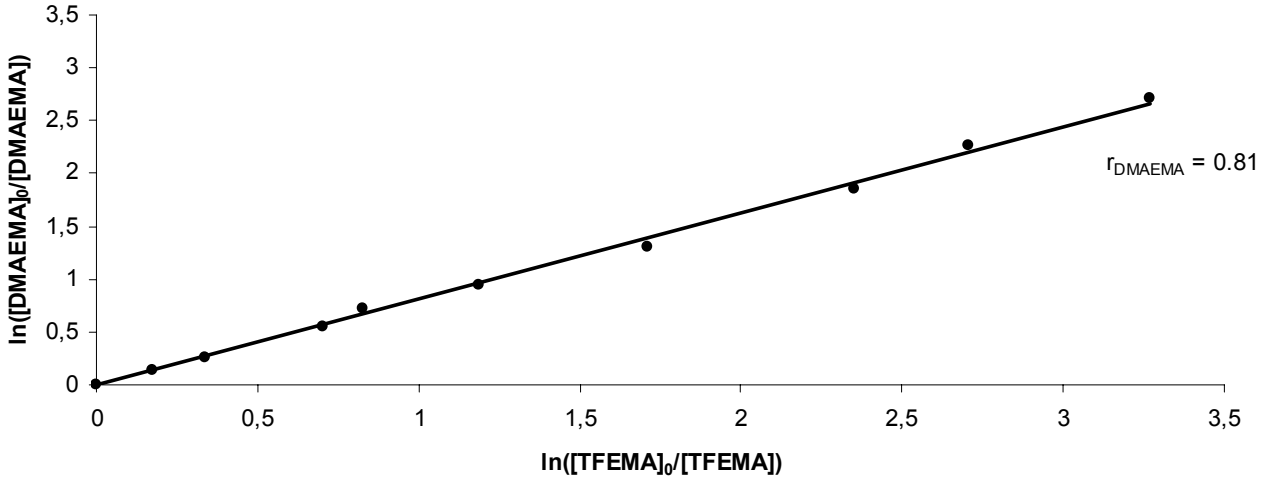


Figure 4. Jaacks plot of the copolymerization of DMAEMA and TFEMA (95:5).

**The exponential decay curves of the spin-spin ($T_2$) relaxation time measurements.**

Each point in the curves represents the height of the $-CF_3$ peak in the $^{19}F$ spectrum, as the number of pulses in the echo train is increased from 2 to 256. The used echo times ($\tau$) are reported for each measurement separately in the figure captions.

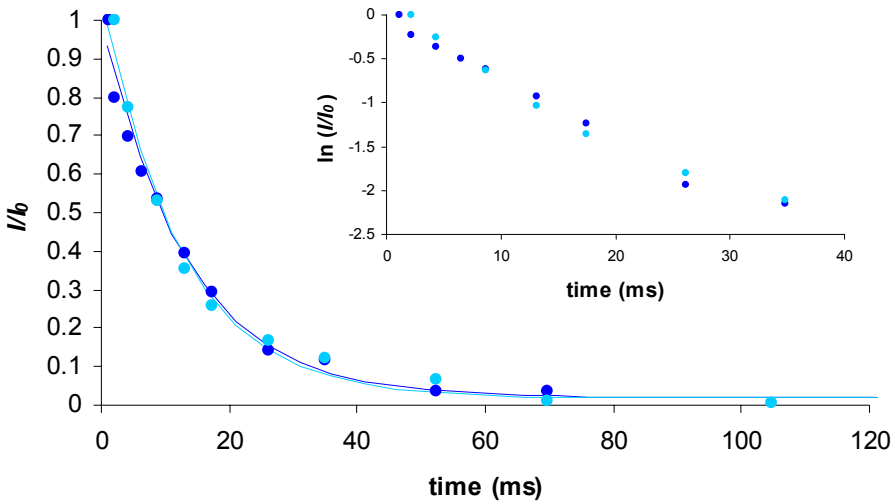


Figure 5. Spin-spin ($T_2$) relaxation time measurements for the 1 w/v-% C-12 solutions at pH 8 with exponential decay curves fitted. Dark blue: no salt, measured with $\tau$ = 250 µs. $T_2$ = 13 ms. Light blue: 0.25 M NaCl, measured with $\tau$ = 500 µs. $T_2$ = 12 ms.

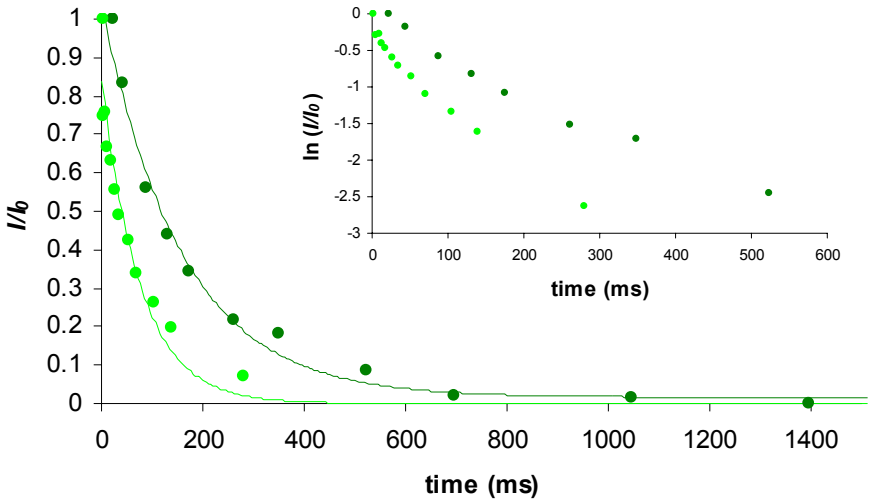


Figure 6. Spin-spin ($T_2$) relaxation time measurements for the 1 w/v-% C-12 solutions at pH 6.5-7.3 with exponential decay curves fitted. Dark green: pH 6.5, no salt, measured with $\tau$ = 5 ms. $T_2$ = 140 ms. Light green: pH 7.3, 0.25 M NaCl, measured with $\tau$ = 500 µs. $T_2$ = 76 ms.

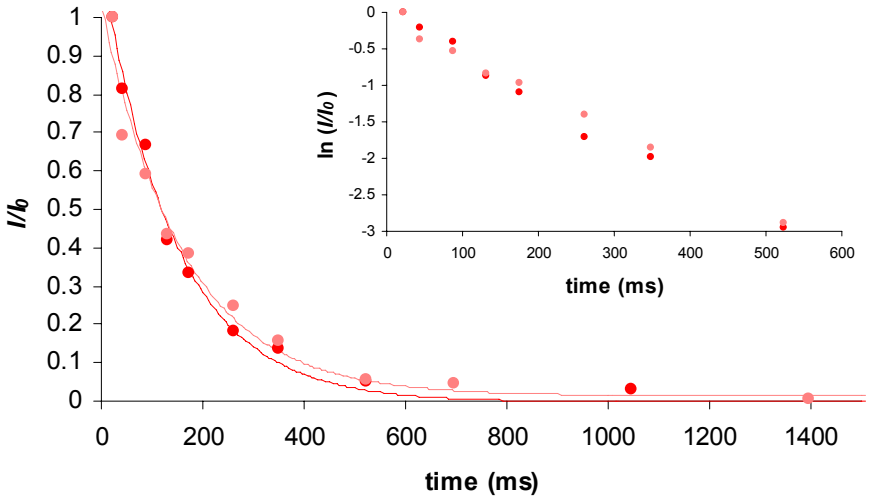


Figure 7. Spin-spin ($T_2$) relaxation time measurements for the 1 w/v-% C-12 solutions at pH 2 with exponential decay curves fitted. Dark red: no salt, measured with $\tau$ = 5 ms. $T_2$ = 140 ms. Pink: 0.25 M NaCl, measured with $\tau$ = 5 ms. $T_2$ = 160 ms.

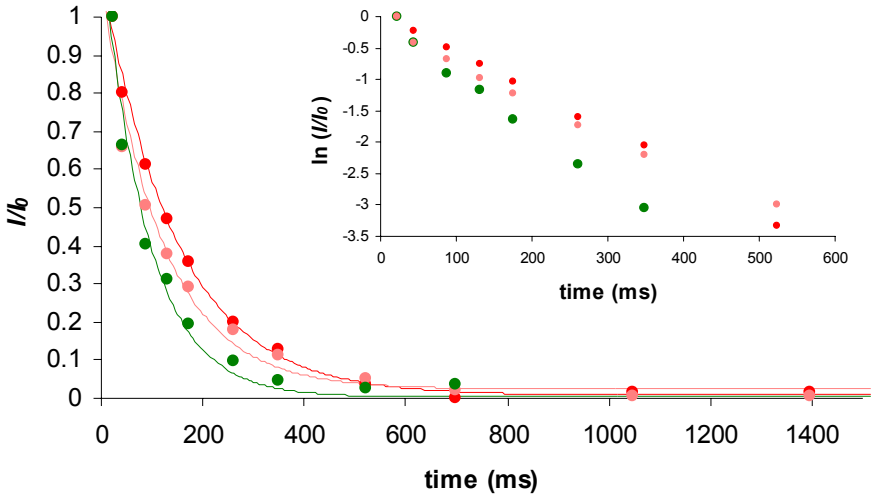


Figure 8. Spin-spin ($T_2$) relaxation time measurements for the 1 w/v-% C-24 solutions with exponential decay curves fitted. Green: pH 6.5, no salt, measured with $\tau$ = 5 ms. $T_2$ = 81 ms. Dark red: pH 2, no salt, measured with $\tau$ = 5 ms. $T_2$ = 150 ms. Pink: pH 2, 0.25 M NaCl, measured with $\tau$ = 5 ms. $T_2$ = 120 ms.

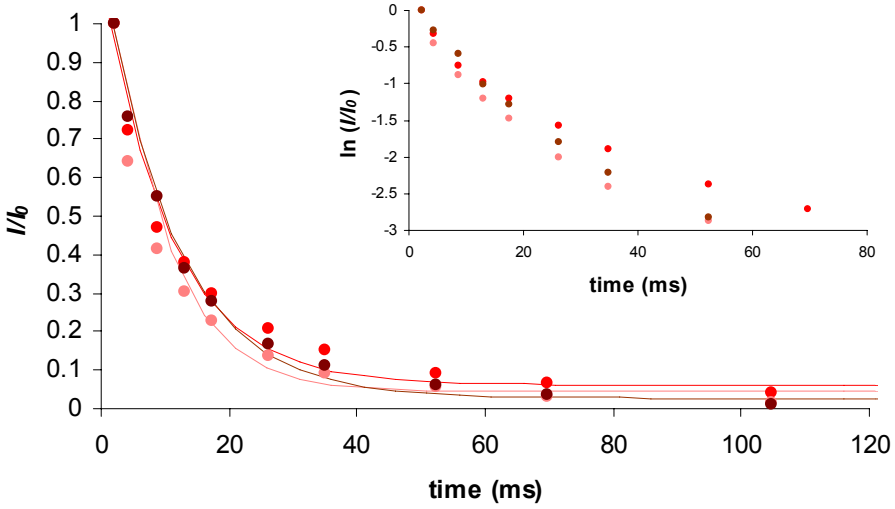


Figure 9. Spin-spin ($T_2$) relaxation time measurements for the 1 w/v-% C-51 and QC-51 solutions with exponential decay curves fitted. Dark red: C-51, pH 2, no salt, measured with $\tau$ = 500 µs. $T_2$ = 11 ms. Pink: C-51, pH 2, 0.25 M NaCl, measured with $\tau$ = 500 µs. $T_2$ = 8.4 ms. Brown: QC-51, 0.25 M NaCl, measured with $\tau$ = 500 µs. $T_2$ = 11 ms.

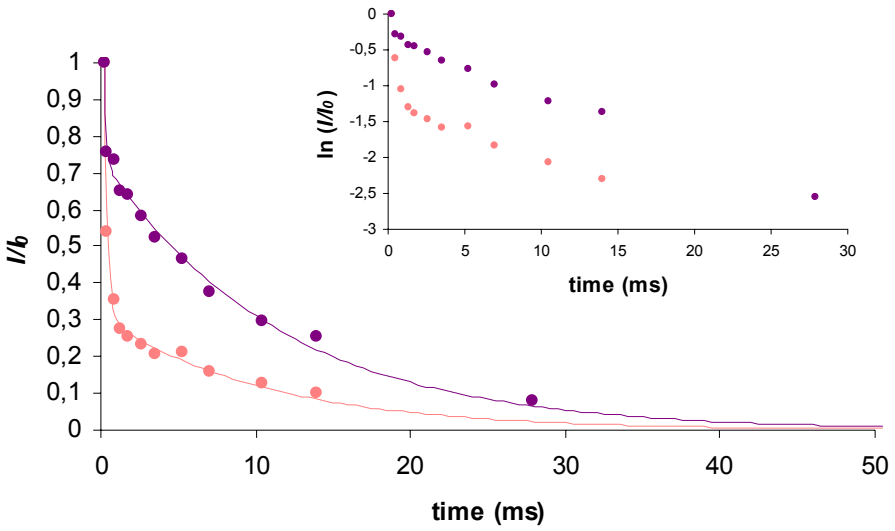


Figure 10. Spin-spin ($T_2$) relaxation time measurements for the 1 w/v-% B-20 and B-47 solutions with exponential decay curves fitted. Purple: B-20, measured with $\tau$ = 50 µs. $T_2$ = 69 % 0.12 ms and 31 % 11 ms. Pink: B-47, measured with $\tau$ = 50 µs. $T_2$ = 86 % 0.22 ms and 14 % 11 ms.

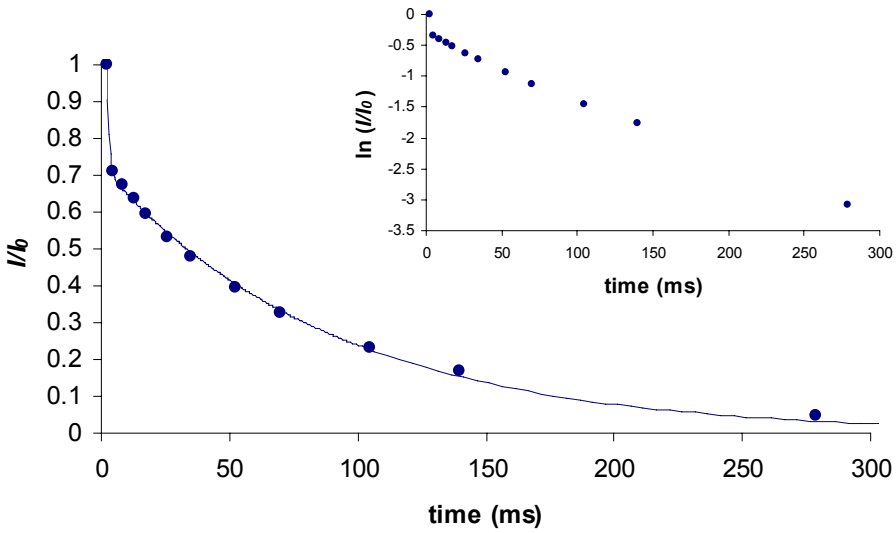


Figure 11. Spin-spin ($T_2$) relaxation time measurement for the 2.5 w/v-% QB-47 solution with exponential decay curve fitted. Measured with $\tau$ = 500 µs. $T_2$ = 89 % 0.73 ms and 11 % 81 ms.

**References**

1 V. Jaacks, *Makromol. Chem.,* 1972, **161**, 161-172 (DOI:10.1002/macp.1972.021610110).

2 S. G. Roos, A. H. E. Muller and K. Matyjaszewski, *Macromolecules,* 1999, **32**, 8331-8335 (DOI:10.1021/ma9819337).

3 I. Ydens, P. Degée, D. M. Haddleton and P. Dubois, *Eur. Polym. J.,* 2005, **41**, 2255-2263 (DOI:10.1016/j.eurpolymj.2005.04.012).